Materials Science-Poland, Vol. 23, No. 4, 2005

Geometrical and electronic properties of ultra thin epitaxial metal nanowires on flat and vicinal Si surfaces

H. PFNÜR*, V. ZIELASEK, CH. TEGENKAMP, T. BLOCK, Z. KALLASSY

Institut für Festkörperphysik, Universität Hannover, Appelstr. 2, D-30167 Hannover, Germany

The study of metallic low-dimensional nanoscale systems requires the generation of ultra-small structures. We demonstrate the feasibility of the formation of metallic wires of arbitrary shape with a lateral width below 10 nm and a thickness from one to several monolayers using a combination of electron beam lithography in ultra-high vacuum and tunnelling microscopy. These methods can be easily combined with surfaces structured by self-organization. As an example, a system consisting of Pb on Si(557) is discussed. It exhibits quasi one-dimensional conduction properties already with one Pb monolayer, which undergoes a temperature-driven structural phase transition, switching the system between high and low conductance anisotropy.

Key words: *low-dimensional nanoscale system; metal epitaxy; nanowires; silver; silicon; electron-beam lithography; tunnelling microscopy; surface conductivity*

1. Introduction

One- or two-dimensional electronic systems are very interesting physical objects, since due to electron confinement, increased electron correlation [1] leads to strong deviations from the Fermi liquid, and in 1D to the formation of a Luttinger liquid [2, 3]. Particularly in one-dimensional systems the enhanced interaction is accompanied by instabilities. Interactions between the lattice, charge, and spin cause the formation of charge and spin density waves lowering the energy and leading to metal –insulator transitions in the electronic transport properties of such systems [1, 4].

Already for ideal systems it is clear that the electronic properties of low -dimensional systems are intimately related to their geometric structure. In real and very small one- or two-dimensional systems, this problem is modified by the fact that they must be supported by or embedded into a substrate material or stabilized by other means. Thus their realizations are always approximate and use either strongly anisot-

*Corresponding author, e-mail: pfnuer@fkp.uni-hannover.de

ropic crystals [5, 6] and polymers [7] or supporting surfaces [8]. Adsorbed layers, which partly form chain structures on substrates like Si(111) [8, 9], are alternative realizations that come closer to atomic chains, and allow precise access to the geometric and electronic properties of quasi one-dimensional systems.

These examples illustrate that realizations of quasi one-dimensional systems are of high interest. In the present paper, we explore two possibilities of realizations. The first is using the top-down approach, i.e. it is an extension of conventional electron beam lithography, which has the potential to provide one-dimensional structures of arbitrary shape. The limit of one-dimensionality, however, is not yet reached at present. We report on our first results of combining electron beam lithography with epitaxy of silver on silicon for the generation of epitaxial metal nanowires on an insulating support. In order to avoid surface contamination induced by the lithographical processes, we employ an *in situ* nanolithography technique for silicon surfaces, developed by Ichikawa and his group, which takes place entirely in ultra-high vacuum. It is demonstrated that this nanolithography technique, in combination with low -temperature silver epitaxy, may generate ultra thin continuous epitaxial metal nanowires with the width below 20 nm.

In the second part of this paper, a further and quite intriguing example of a bottom-up approach, i.e. the self-organized generation of strongly anisotropic metallic nanostructures in the Pb/Si(557) system, is discussed. The Si(557) surface as a substrate already has a striped wire-like structure with the alternation of (111) and (112) oriented micro-facets, which seems to be almost unchanged by the adsorption of lead. Thus, electronic and geometrical properties can be well compared with those obtained on a flat Si(111) substrate, for which magnetoconductance and correlation with geometric properties have been recently studied extensively [10–13]. The (557) surface is able to superimpose its symmetry onto the adsorbed Pb layer, which, after appropriate treatment, forms chain structures, so that transitions between one- and two-dimensional behaviour can be studied with this system. Even after Pb adsorption, the Fermi level is pinned close to a mid-gap position [14], so that the underlying Si interface is always depleted of charge, irrespective of doping. Here we present temperature-dependent macroscopic DC conductivity measurements in the coverage range between submonolayers up to several layers of Pb obtained after different steps of annealing.

2. Experimental

UHV-lithography experiments were carried out in ultrahigh vacuum (base pressure below 3×10^{8} Pa) in a combined scanning electron microscope (SEM) – scanning tunnelling microscope (STM) system (JEOL SPM 4500 SX). Both microscopes are confocal and can be operated simultaneously at variable sample temperatures in the range 60–900 K. While the electron gun (1–25 keV) provides an SEM resolution of 4 nm, an eucentric tilting mechanism of the sample stage renders it possible to vary the an-

gle of incidence of the electron beam between 0 and 30º (Fig. 1). At glancing incidence, microprobe reflection high-energy electron diffraction (μRHEED) may be used to check the crystallinity of the generated structures. Any diffraction spot may be chosen as an input signal for scanning reflection electron micrographs (SREM). An additional electron energy analyser was used for the Auger electron spectroscopy

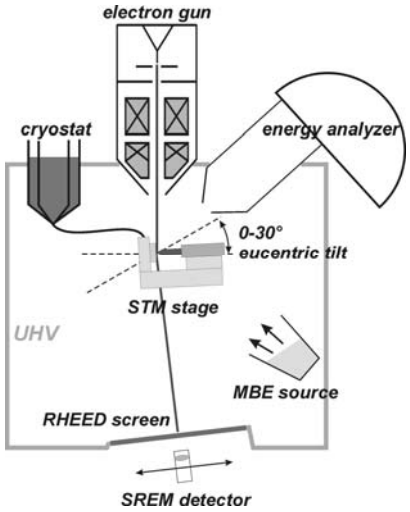

Fig. 1. Schematic drawing of the SEM-STM. This setup also allows scanning Auger microscopy (SAM), electron diffraction at sample areas of the beam diameter (RHEED), and scanning microscopy with the reflected electrons (SREM). Sample temperature can be varied in the range 60–900 K during measurements

(AES) and scanning Auger electron microscopy (SAM). The Si(111) substrate samples, sized 0.3×1.5×7 mm^3, were cut from wafers of high resistivity (>1000 Ω·cm). The substrate surfaces were prepared by repeated flash heating to 1400 K by direct current while keeping the ambient pressure below 1×10^{-7} Pa. To oxidize the surface, the sample temperature was raised to 943 K for 10 min after oxygen (99.999%) was introduced into the chamber at a pressure of 2×10^{-4} Pa. It has been demonstrated that a complete layer of oxide 0.3 nm thick is formed under these conditions [15–17]. Surface quality and contamination were monitored by STM, RHEED, and AES. Silver was evaporated from a well-outgassed Knudsen cell. The deposition rate was determined using a quartz microbalance calibrated via STM measurements. For calibration, Ag was deposited in submonolayer amounts onto the substrate held at the temperature of 700 K. The areal fraction of Si(111) ($\sqrt{3}\times\sqrt{3}$)R30°–Ag regions was determined and the Ag coverage calculated, assuming the density of 1 Ag atom per Si atom of the topmost layer (7.83×10^{14} cm^{-2}) in the ($\sqrt{3}\times\sqrt{3}$)-reconstructed regions, according to the HCT model [18].

Experiments with Pb on Si(557) were carried out again under ultra-high vacuum conditions in two separate vacuum chambers, set up for conductivity measurements at variable temperatures down to 3.5 K (apparatus A), and for tunnelling microscopy at variable temperatures down to 40 K (apparatus B). In both chambers, the average morphology was controlled by low energy electron diffraction (LEED), and the cleanliness of the Si surfaces by STM and by Auger spectroscopy (AES). The Si(557)

substrates (Crystec, Berlin) were chemically cleaned ex-situ. Atomically clean Si(557) surfaces were obtained by removing the native oxide by evaporation of Si at a surface temperature of 1170 K instead of using high temperatures [19]. The Pb coverage was calibrated by conductivity measurements of thick Pb films grown on Si(111) substrates at 20 K [11] within the accuracy of 5% of a monolayer (ML).

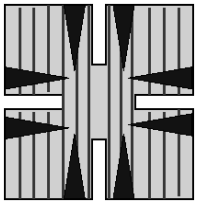

Fig. 2. Schematic of Si(557) samples prepared for DC conductance measurements via the eight $TiSi_2$ contact pads (marked by dark triangles). The lines indicate the stripe structure along the $[1\bar{1}0]$ direction

In our experiments, an extended four-point probe technique was used to conduct measurements (Fig. 2). The sample had eight pre-deposited macroscopic $TiSi_2$ contacts with a thickness of approximately 50 nm, which were separated pairwise by slits machined into the samples as shown in Figure 2. The separation between equivalent contacts was approximately 10 mm. Details about experimental procedures, thickness calibration, etc. can be found in ref. [20].

3. UHV electron beam lithography

3.1. Generation of Si(111)/Si oxide templates

The lithographical process used in order to form clean silicon windows within an oxide mask is shown in Figure 3, and has been described in detail by Ichikawa and

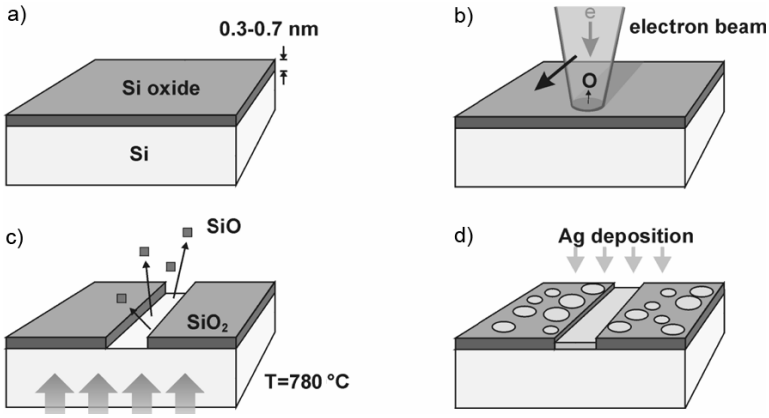

Fig. 3. E-beam lithography in UHV for the generation of silver nanostructures on silicon: a) thin thermal oxide on Si, b) electron-induced oxygen desorption in selected areas, c) void formation in the oxide via thermal desorption of SiO, d) Ag deposition leading to cluster formation in oxide areas and epitaxial Ag layers in the Si window

co-workers [21, 22]. An oxidized Si sample is irradiated with the electron beam of the SEM, thus partially reducing the SiO_2. Heating the sample to temperatures below the desorption temperature of SiO_2 leads to electron-beam induced selective thermal decomposition and the desorption of substoichiometric oxide. The width of the silicon windows depends on the primary electron dose and on the duration of subsequent heating. The total electron dose has to be optimised in order to obtain continuous Si windows while maintaining a good lateral resolution, as the plume of secondary electrons damages the oxide around the focus of the primary electron beam. In our experiments, the sample surface was irradiated at an angle of ca. 10° with respect to the surface plane, with a total surface electron dose of 100–200 C/cm^2 and an electron energy of 25 keV. After electron irradiation, the surface was heated up to 780 °C for 10–30 s. Besides the desorption of SiO, the etching of SiO_2 by bared Si leads to the decomposition of the oxide [17], which is seen by the continuous propagation of the oxide boundary and widening of the Si windows during prolonged heating. STM has demonstrated that the Si surface in the window areas is atomically clean.

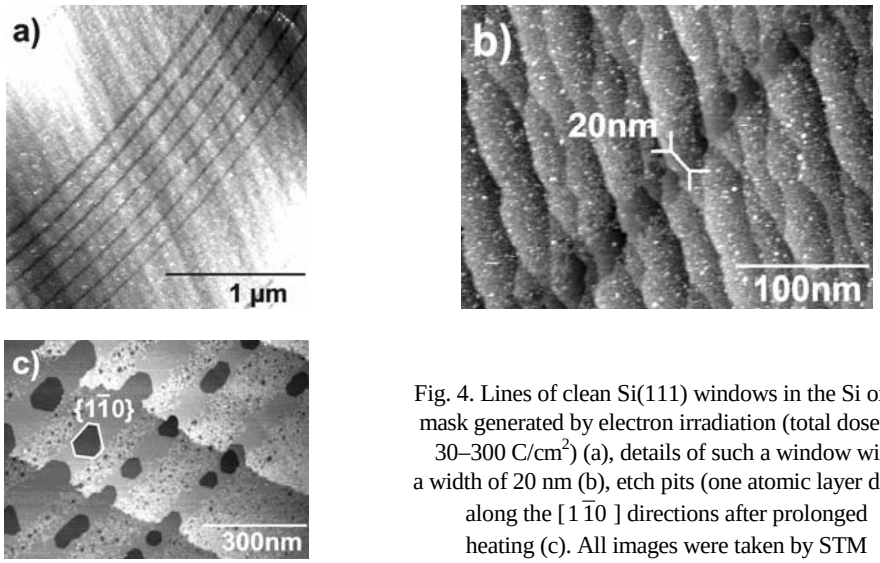

Fig. 4. Lines of clean Si(111) windows in the Si oxide mask generated by electron irradiation (total doses of 30–300 C/cm^2) (a), details of such a window with a width of 20 nm (b), etch pits (one atomic layer deep) along the [1 $\bar{1}$0] directions after prolonged heating (c). All images were taken by STM

Figure 4 shows line-shaped Si(111) windows, which were generated as templates for silver nanowires. With electron doses and the subsequent heating procedure optimised, the windows are continuous over a distance of several micrometers (Fig. 4a). We have generated the windows as narrow as 7 nm, while windows with the width of 20 nm as shown in Figure 4b are achieved regularly, also on substrates with a high step density, where the boundaries between oxide and windows often appear less sharp than on large single terraces. Figure 4c shows the result of prolonged heating after electron irradiation. The consumption of silicon from the bared areas during the decomposition of the oxide is evident by etch pits, which form especially at atomic steps, but also on flat Si(111) terraces in the window areas. The etch pits are one

atomic layer deep and their borders are probably aligned along the $[1\bar{1}0]$ directions, as observed, e.g., for Si(111) etching by water [23].

3.2. Ag epitaxy

The deposition of silver is the next step in the lithographical process. On bare silicon surfaces, silver grows epitaxially without forming silicides, making silver an ideal candidate for insulated metal nanostructures on silicon with a well-defined interface between metal and substrate. Silver on Si(111) exhibits a variety of growth modes. At room temperature, silver grows on Si(111) in the Stranski–Krastanov mode [24]. For silver deposition at low temperatures (<170 K) and various annealing procedures, however, a variety of metastable structures have been reported as a result of limited kinetics. STM studies have shown that silver grows layer by layer and is atomically flat at a sample temperature of 100 K [25].

Layer by layer growth has also been observed for deposition at 150–170 K [26]. With an increasing amount of the deposited material, interconnected islands, flat islands on top of a rough wetting layer, and continuous Ag layers have been observed when the surfaces were annealed to room temperature after deposition [27]. For the flat islands, preferred island heights have been identified. While the reason for the occurrence of different preferred heights in seemingly similar experiments (2 ML [26, 27, 28] and 6 ML [29]) has not been clarified yet, these magic heights are ascribed to the contribution of electron confinement within the metal layer to its free energy [28]. Spot profile analysis of LEED has shown that the continuous films consist of atomically flat grains, forming a small-angle (6°) rotational mosaic [30]. Grain diameters in the range 1.5–9.5 nm have been observed, depending on the substrate temperature during deposition and annealing.

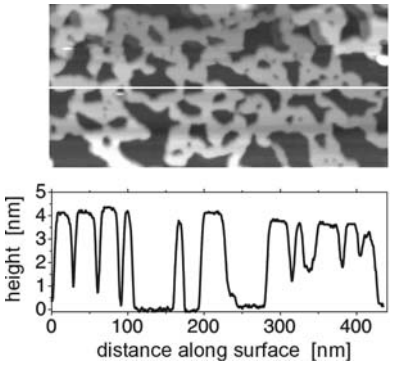

Fig. 5. STM of 10 ML of Ag on homogeneous Si(111) deposited at 130 K and annealed to room temperature. A percolated network of flat Ag islands is seen. Bottom: the line scan shows the narrow range of island heights around 4 nm

As an example from own measurements, Figure 5 shows an STM image of 10 ML Ag on a Si(111) substrate with a low step density and wide terraces in the range of 100 nm. The silver layer was deposited at 130 K and annealed to room temperature. Instead of a continuous Ag layer, we find a percolated network of islands, obviously

aligned along the low index directions of the substrate lattice (the STM image in Figure 5 is not corrected for thermal drift). The islands all have about the same height of 4 nm, with a variation of not more than ±15%, as shown by the line scan in Figure 5.

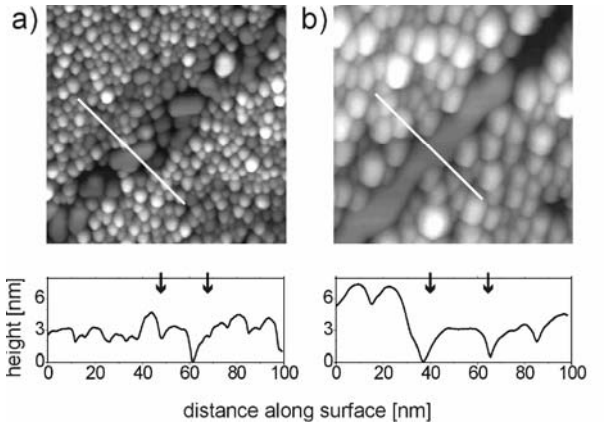

Fig. 6. STM images (size 150×150 nm^2) of 7 ML Ag deposited at 130 K on an Si(111) window in an oxide mask and annealed to a) 300 K and b) 700 K. Line scans along the white lines are shown below the STM image; 3 nm high Ag islands are seen in the window areas (borders of the window areas are marked by arrows). Sample bias –8 V, tunnelling current – 45 pA

Such a percolated network of islands of uniform height in a line-shaped Si window within an oxide mask would make a perfect nanowire. Figure 6a shows 7 ML Ag deposited on a Si(111)/Si oxide template at 130 K and annealed to room temperature. On the oxide area, spherical Ag nanoclusters have formed. The low surface free energy of the oxide surface inhibits the metal to wet the oxide. In the line-shaped Si(111) window, separate flat epitaxial islands with diameters in the range of 10–20 nm are detected. Obviously the growth mode in the narrow Si(111) window differs from that on bare Si(111), either due to defects such as nucleation sites or due to additional kinetic limitations. Apparently there is no significant transport of silver from the oxide area to the silicon window and vice versa. All material hitting the oxide area is consumed by the clusters. When the diffusion of silver atoms is restricted to the line-shaped Si(111) window, any coarsening of islands may be hindered.

Figure 6b shows the result of annealing 7 ML Ag deposited at 130 K on a line-shaped Si(111)/Si oxide template up to about 700 K. Comparison with Figure 6a reveals that the clusters on the oxide have coarsened. They still appear to be spherical in shape, indicating that they are not interconnected. Within the Si(111) window, a single elongated island has formed. The line scan depicted underneath the STM image reveals that the island is about 3 nm high, has a flat top, and is separated from the adjacent clusters in the oxide area.

Such nanowire sections have been observed with a total length up to 250 nm in our STM experiments. Figure 7 shows two nanowire sections with the width of 15–25 nm in adjacent Si(111) windows. The disturbances visible in the STM image are due to tip

changes, presumably induced by the detachment or attachment of silver atoms. Figure 7 also shows two islands in an 80 nm wide Si(111) window. Their lateral shape

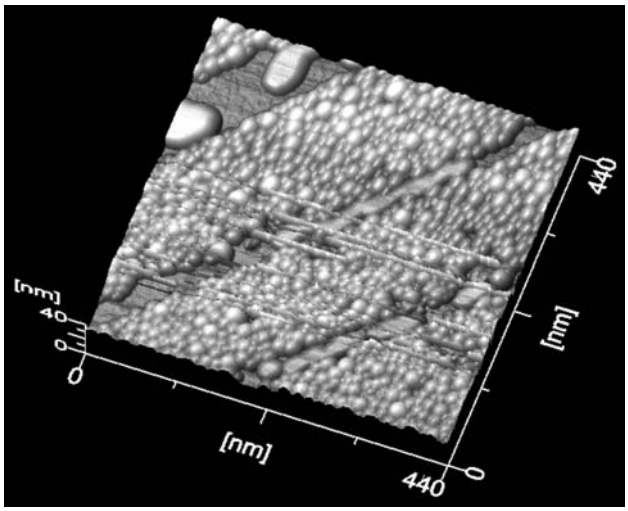

Fig. 7. A demonstration of wire-shaped Ag islands on an Si(111)/Si oxide mask in a narrow Si window (20 nm wide), and of 2D Ag islands in the wider window (80 nm)

appears as round as it is expected for silver deposition on bare silicon. Obviously, the tendency to form elongated nanowire sections is promoted by narrow Si windows. The role of the interface between the Si window and the oxide for Ag diffusion and the nucleation of Ag islands have not been investigated yet.

3.3. Ag wetting layer

Besides the 3 nm high nanowire sections, the Ag wetting layer in the Si(111) windows may be regarded as a metal nanowire in its own right. A surface state conductance in the range of $(5–10)\times10^{-5}\,\Omega^{-1}$ has been reported [31]. The $(\sqrt{3}\times\sqrt{3})R30^{\circ}$-Ag surface has a metallic surface state band as demonstrated by the observation of standing electron waves [32] and a two-dimensional plasmon [33]. It is particularly interesting, since, in contrast to the nanowire sections shown above, the wetting layer is limited in length only by the size of the Si(111) window. It is generated by annealing silver on Si(111) up to 700 K or by depositing at that temperature, and is composed of $(\sqrt{3}\times\sqrt{3})R30^{\circ}$-Ag domains [34].

Figure 8 shows the wetting layer formation in line-shaped Si(111) windows within an oxide mask. While only 0.5 ML Ag was deposited on the surface (deposition temperature 790 K, rate 0.13 ML/min) the window area is completely covered by the wetting layer, indicating Ag diffusion from the oxide to the window area. Pits due to

an Ag-induced surface reconstruction as well as islands of an additional layer can be seen in the window areas. The observed height differences within the windows always correspond to multiples of the Si(111) bilayer thickness. This observation indicates that the Si substrate is completely covered by the wetting layer, because the height difference between (7×7) and adjacent ($(\sqrt{3}\times\sqrt{3}$)-Ag terraces would clearly differ from the Si bilayer thickness.

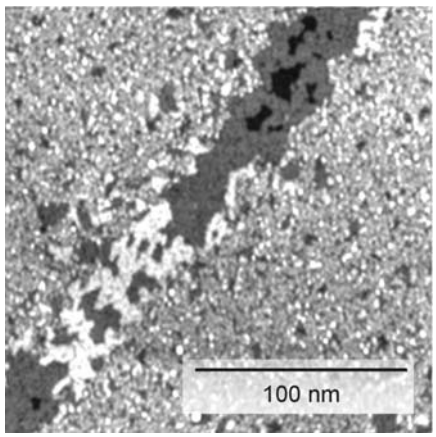

Fig. 8. STM image of 0.5 ML Ag deposited on a Si(111)/Si oxide template at 790 K at the rate of 0.13 ML/min. Due to migration from the surrounding oxide film, the Si window is covered by a continuous Ag wetting layer. In some parts (bright areas), a second Ag layer starts to grow

Concluding this section, we have shown that ultra thin crystalline metal nanostructures with characteristic lateral dimensions of much less than 20 nm can be generated on an insulating support using a combination of electron beam lithography in ultra-high vacuum and Ag epitaxy on Si(111). Details of the morphology of the metal deposit depend partly on the lateral constriction imposed by the oxide mask. Various thicknesses can be exploited starting with the wetting monolayer. Arbitrary shapes have not been tested explicitly yet, but seem to be easily feasible.

4. Conductance of Pb on Si(557) in the monolayer regime

In the Pb/Si(557) system, we start with a macroscopic measurement (distance between contacts was 10 mm, as already mentioned) of conductance on Si(557) samples that were prepared as described in the experimental section. For Pb layers evaporated onto the Si(557) samples at low temperature (below 25 K), the onset of measurable Pb-induced conductance was found to be close to 0.6 ML (ML given with respect to the density of Si surface atoms). Annealing to temperatures up to 600 K leads to an increase in conductance (except at coverages close to the percolation threshold, at which no effect was detected) and to the reversibility of conductance as a function of temperature. It is characterized by a weak anisotropy, with conductance normal to the steps being smaller by typically a factor of 1.5 than that perpendicular to them.

4.1. Conductance of an anisotropic Pb monolayer

This behaviour of a weak anisotropy and a gradual increase in conductance as a function of temperature is changed drastically by an annealing step to 640 K. The curves obtained after this high-temperature annealing step are now dominated by an abrupt change at the temperature of 78 K, separating a high-temperature region with small conductance anisotropy (ratio 1.5) from the low-temperature region characterized by high anisotropy (ratio 30–60). At temperatures below 78 K, a stepwise increase of $\sigma_{\parallel}$ by typically a factor of 3 is observed, whereas $\sigma_{\perp}$ drops sharply by a factor of 2–10. This final step of annealing obviously induces two effects. The monolayer undergoes an ordering process that is strongly activated, so that it occurs only during annealing to temperatures close to desorption. The alternative that a mixing of Si and Pb atoms in the first layers takes place, so that a surface silicide is formed, is unlikely judging by the STM data presented below.

The switching of conductance from low to high anisotropy was found to be independent of the initial Pb coverage, Θ_{ini}, after the high-temperature annealing step to 640 K, if it exceeded 1 ML. An example, with Θ_{ini} = 4 ML and annealing to 640 K, is shown in Figure 9. The vapour pressure of bulk Pb at 640 K is 7×10^{-7} mbar [35]. This means that after annealing for several minutes all multilayers of Pb must have been desorbed, directly explaining the insensitivity of the conductance results to the initial coverage in the multilayer range after the high-temperature annealing step. The fact that conductance can be switched, driven by temperature, from high to low anisotropy is therefore a property of the monolayer of Pb and/or of the conductance channels induced by the Pb monolayer on the Si(557) surface. The assumption of monolayer coverage is fully compatible with the STM results described below. As seen there, atomic wire-like structures are formed after this high-temperature annealing step, which are responsible for the anisotropy of the conductance observed at low temperature.

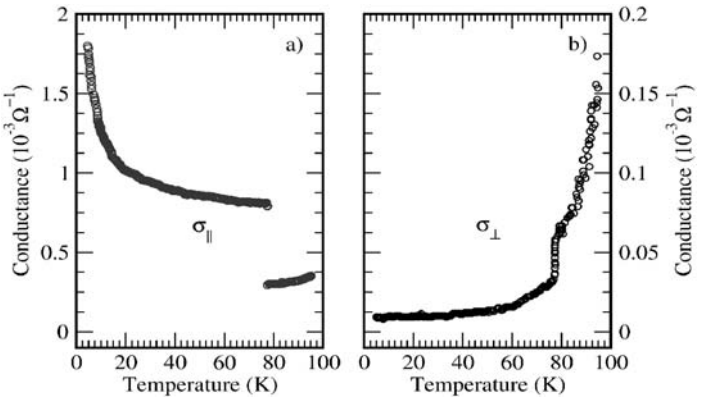

Fig. 9. DC conductance as a function of temperature after the adsorption of 4 ML and annealing to 640 K, measured along the [112] ($\sigma_{\perp}$) and [110] direction ($\sigma_{\parallel}$)

For the "optimal" conductance curves after annealing, i.e. those obtained with initial Pb coverages of 3ML or more, $\sigma_{\parallel}$ below T_c can be well described by $\sigma_{\parallel} = A + B \times T^{-n}$, with n close to 1 (see Fig. 10). This decrease of $\sigma_{\parallel}$ as a function of temperature contrasts with the increase above the jump at 78 K, indicating thermally activated behaviour above this threshold. $\sigma_{\perp}$, on the other hand, is thermally activated in both temperature regimes. Whereas for $\sigma_{\perp}$ defects may play some role as mentioned, the optimal conductance values of $\sigma_{\parallel}$ did not vary between different samples, and neither the abrupt changes seen in the conductance at 78 K nor the temperature dependence of $\sigma_{\parallel}$ below 78 K can be explained by defects. While we cannot expect that a surface is free of defects like point defects or steps, at least on the atomic scale, such defects cannot act as effective scatterers along Pb chains.

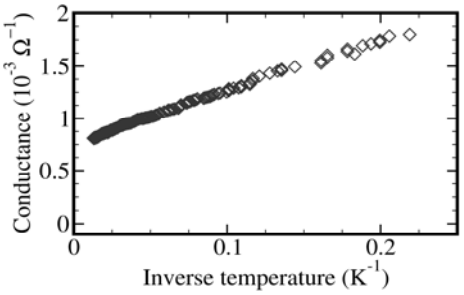

Fig. 10. Conductance curve $\sigma_{\parallel}$ from Fig. 9 below 78 K plotted versus $1/T$

This property changes when the coverage is so small that only very few chains are left, which form a conducting channel between the contacts of our experimental setup. Here there is a high probability for more extended defects that can only be surmounted by thermal activation. This scenario seems to be valid at a Pb concentration of 0.8 ML and lower. The observed jump in conductance at T_c and the increase of $\sigma_{\parallel}$ as a function of temperature below T_c is compatible with the assumption of sections of isolated chains separated by gaps, which can still be surpassed by thermal activation.

4.2. Conductance and geometrical properties

The clean Si(557) surface (not shown) corresponds closely to that shown in Ref. [36]. These results are supported by LEED, which shows the characteristic 7×7 reconstruction of (111) facets [37, 38] and the known 2×1 reconstruction of Si(112) surfaces [39]. Microscopically, the (111) facets are separated by 3-fold steps. The typical terrace lengths that can be obtained on our samples are around 200 nm. Neighbouring (111) terraces are separated by steps that correspond to steps of 6 and 9 atomic heights. Kinks in the step edges can also be seen. In any case, these extended line defects remain on the atomic level. Even with a low density of terraces, many thousand steps intersect the path between two contacts in our experimental setup.

As judged from a large series of adsorption experiments and various annealing steps, adsorbed Pb leaves the terrace structure of the Si(557) sample unaltered. After

the adsorption of Pb at low temperatures and annealing for 15 minutes at 640 K, STM reveals the characteristic chain structure shown in Figure 11, with an average spacing between the chains of 14 Å. This chain structure is found only after the high-temperature annealing step, whereas a more irregular bumpy hill-and-valley structure is found at lower annealing temperatures. The chain structure is destroyed by annealing at 650 to 660 K. Thus there is a close correlation between the chain structure observed here and the strongly anisotropic conductance behaviour found below 78 K at one monolayer coverage. The surface shown in Figure 11 is completely covered with Pb, and all chain structures are Pb-induced.

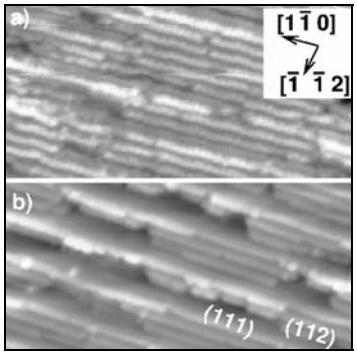

Fig. 11. STM images (40 ×20 nm^2) of the chains after the adsorption of 10 ML Pb/Si(557) and annealing to 640 K. The temperatures of measurement were a) 40 K and b) 100 K

It seems that two different kinds of chains on the surface can be discriminated, which may be attributed to chain formation on the two facets. As judged from chains ending at small clean 7×7 islands, the bright chains must be located on the (111) facets or at the edge between the two facets, whereas the other chains must be on the (112) facets. The step-step distance there is around 10 Å on the clean surface, i.e. it is significantly smaller than the Pb–Pb chain separation. This enlarged chain distance can be caused by effective lateral repulsion between wires, so that they are not located at equivalent positions on each mini-terrace, supporting the assumption of coupled chains. As an alternative, step separations on the original (112) facets, induced by Pb and high-temperature annealing, could be enlarged at the expense of the extension of the (111) facet. If this rearrangement of the local step structure is necessary, it would explain the necessity for high-temperature annealing. In any case, it is obvious that each Pb wire consists of more than one atomic chain in order to accommodate a Pb concentration of approximately 1 ML. Even at a temperature of 40 K these chains contain a lot of defects that limit the typical undistorted length of a chain to 30–100 nm, with the bright chains containing typically less defects than the others. Whereas the chain separation has a well-defined value, the stacking sequence normal to the chains seems to follow the local variation of facet sizes, so that it is not long range ordered.

The abrupt changes observed at T_c = 78 K are directly correlated with an intriguing structural phase transition that does not change the chain structure itself, as seen in Figure 11a, b (the images there were taken at 40 K and 100 K, respectively, i.e. below and above the phase transition). The effects associated with the phase transi-

tion, however, are most clearly visible in one-dimensional Fourier transformations along and perpendicular to the chain structures. The results are shown in the top part of Figure 12 for a typical single scan. Averages over an area of 40×40 nm^2 are shown in a log scale in panels a) and b) of this figure.

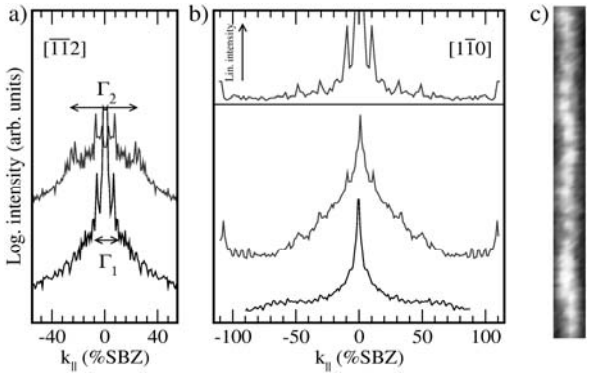

Fig. 12. Fourier transformations of line scans from STM pictures at 100 K (lower curves) and at 40 K for the direction perpendicular (a) and parallel (b) to the steps. The top graph of b) shows the Fourier transform of a single atomic chain in a linear scale. Such a chain is shown in c) in real space.

In the direction normal to the chains (left part of Fig. 12), for both temperatures, a clearly enhanced Fourier component Γ_1 is seen, which corresponds to an average hill and valley spacing of 57 Å, i.e., to the periodicity of the clean Si(557) surface. For T = 40 K an additional, but considerably broader component Γ_2 is seen, which corresponds to the 14 Å spacing of the Pb wires.

Parallel to the chain structure the Fourier transforms calculated from 40 K STM images show, in contrast to those of STM images taken 100 K, an additional periodicity with a fundamental wavelength of 10 times the next neighbour separation of Si, along with higher harmonics. The peak at 110% SBZ corresponds to the nearest -neighbour spacing of Pb with approximately the bulk Pb lattice constant. Little correlation of this periodicity between different chains was found. The modulation of the chains is weak, as is obvious from Figures 11 and 12. It cannot be induced by missing Pb atoms, as seen, e.g., for the case of Ga on Si(112) [40], but rather by a modulation of the local position of adatoms, most likely due to the misfit between Si and Pb lattice constants. Since the lattice constant of Si is 9% larger than the lattice constant of Pb, registry between the ideal Si and Pb lattices is obtained every ten Si atoms, which agrees well with the ten-fold periodicity found.

Approaching T_c from higher temperatures, it seems to be the locking of the chains into the high order commensurate superperiodicity, coupled with a regular separation between the Pb induced chains, that causes the switching from low to high anisotropy and into a highly conducting state along the chains with a “metallic”-like temperature dependence.

Electrical conduction in this system occurs in the partially filled band of Si surface states, which is modified by the adsorbed Pb chains that impose their symmetry and their periodicity onto this band. As judged from the low electrical conductivity in the $[1\bar{1}0]$ direction in the low temperature regime and its temperature dependence, coupling is rather weak between the chains, and the electrons close to E_F are preferably localized within one chain. Along the chains, the 10-fold periodicity imposes a mesoscopic modulation that effectively backfolds the band structure of the unmodulated chains. Thus the effective Fermi wavelength λ_F cannot be smaller than twice the modulation period, but may be even much longer. The corresponding effective increase of λ_F can rationalize why these electrons are quite unsusceptible to local defects on the atomic scale along the chains. Although defects are present, they do not lead to the localization of the conducting electrons along the wires down to temperatures of 4 K.

Passing the phase transition, the conductance normal to the Pb chains drops sharply, but here the activated temperature behaviour seen above the phase transition remains also at temperatures below. This strong anisotropy means a strongly enhanced localization of the electrons in the direction normal to the wires, which is destroyed at higher temperatures when the spatial correlation between the wires is lost. We note that above the phase transition both $\sigma_{\parallel}$ and $\sigma_{\perp}$ return to activated behaviour, i.e., to an increased sensitivity to local defects. This fits qualitatively to the model of a much shorter effective λ_F in both directions in the high-temperature phase than at low temperatures.

The conductance behaviour in the highly anisotropic state may be a candidate for Luttinger liquid behaviour in coupled chains [41]. Since we observe quasi one-dimensional conductivity down to 4 K, the energy scales for two-dimensional coupling are extremely small (of the order of a few kelvin or even less) compared to standard quasi one-dimensional conductors [42]. This suggests that we have found a system with almost ideal one-dimensional conductive properties. On the other hand, the quantitative properties deviate clearly from predictions for DC conductance in a Luttinger liquid, even in the presence of defects [43], since a rather high background must be subtracted from the data in order to obtain a simple power law. The meaning of the (still one-dimensional) "background" conductance must remain open at this point. Significant coupling between the chains must also exist, as indicated by the nonzero value of $\sigma_{\perp}$ and its increase as a function of temperature [42, 44]. Whether defects such as additional steps are important for these deviations cannot be answered at the moment.

Summarizing, our results show that quasi-metallic quasi one-dimensional conductance with extremely high values of conductance can be obtained with only one monolayer of Pb that forms a chain structure on Si(557). Conductance can be switched from low to high anisotropy by an order-disorder phase transition with a mesoscopic modulation period. Thus, and in strong contrast to the metal-insulator transitions seen in most systems when temperature is decreased, we observe transi-

tions from a quasi one-dimensional metal at low temperature to an insulator (with temperature-activated behaviour) at high temperature parallel to the Pb chains, and an insulator–metal transition in the direction normal to the Pb chains.

Both sets of experiments described in this paper emphasize the power of ultimate nanostructuring for gaining new insight into the physics of low-dimensional systems. Especially the role of defects must be clarified in further experimental studies on a very small scale, so that individual defects and their influence on conductance can be directly detected. Such experiments seem to be feasible with such nanoscale techniques.

References

[1] VOIT J., Rep. Prog. Phys., 58 (1995), 977.
[2] LUTTINGER J.M., Phys. Rev., 119 (1960), 1153.
[3] HALDANE F.D., J. Phys. C. Solid State Phys., 14 (1981), 2585.
[4] PEIERLS R.E., *Quantum theory of solids*, Clarendon, Oxford, 1955.
[5] JEROME D., Chemica Scripta, 17 (1981), 13.
[6] CLAESSEN R., SING M., SCHWINGENSCHLÖGL U., BLAHA P., DRESSEL M., JACOBSEN C.S., Phys. Rev. Lett., 88 (2002), 096402.
[7] ROTH S., GRAUPNER W., Synthetic Metals, 57 (1993), 3623.
[8] HIMPSEL F.J., ALTMANN K.N., BENNEWITZ R., CRAIN J.N., KIRAKOSIAN A., LIN J.-L., MCCHESNEY J.L, J. Phys. C, 13 (2001), 11097.
[9] TANIKAWA T., MATSUDA I., KANAGAWA T., HASEGAWA S., Phys. Rev. Lett., 93 (2004), 016801.
[10] PETKOVA A., WOLLSCHLÄGER J., GÜNTER H.-L., HENZLER M., Surf. Sci., 482–485 (2000), 922.
[11] PFENNIGSTORF O., PETKOVA A., GÜNTER H.-L, HENZLER M., Phys. Rev. B, 65 (2002), 045412.
[12] VILFAN I., HENZLER M., PFENNIGSTORF O., PFNÜR H., Phys. Rev. B, 66 (2002), 241306.
[13] VILFAN I., PFNÜR H., Eur. Phys. J. B, 36 (2003), 281.
[14] RICCI D.A., MILLER T., CIANG T.-C., Phys. Rev. Lett., 93 (2004), 136801.
[15] WATANABE H., KATO K., UDA T., FUJITA K., ICHIKAWA M., KAWAMURA T., TERAKURA K., Phys. Rev. Lett. 80 (1998), 345.
[16] MATSUDO T., OHTA T., YASUDA T., NISHIZAWA M., MIYATA N., YAMASAKI S., SHKLYAEV A.A., ICHIKAWA M., Appl. Phys., 91 (2002), 3637.
[17] MIYATA N., WATANABE H., ICHIKAWA M., Phys. Rev. Lett., 84 (2000), 1043.
[18] KATAYAMA M., WILLIAMS R., KATO M., NOMURA E., AONO M., Phys. Rev. Lett., 66 (1991), 2762.
[19] CZUBANOWSKI M., TEGENKAMP C., PFNÜR H., Appl. Phys. Lett., 84 (2004), 350.
[20] TEGENKAMP C., KALLASSY Z., GÜNTER H.-L., ZIELASEK V., PFNÜR H., Eur. Phys. J. B, 43 (2005) 557.
[21] MARUNO S., FUJITA S., WATANABE H., ICHIKAWA M., J. Appl. Phys., 82 (1997), 639.
[22] FUJITA S., MARUNO S., WATANABE H., ICHIKAWA M., J. Vac. Sci. Technol. B, 16 (1998), 2817.
[23] PIETSCH G., KÖHLER U., HENZLER M., Chem. Phys. Lett., 197 (1992), 346.
[24] LOENEN E.V., IWAMI M., TROMP R., VAN DER VEEN J., Surf. Sci., 137 (1984), 1.
[25] MEYER G., REIDER K.-H., Appl. Phys. Lett., 64 (1994), 3560.
[26] KIMBERLIN K., RUTTER G., NAGLE L., ROOS K., M.TRINGIDES, Surf. Interface Anal., 35 (2003), 1069.
[27] JIANG C.-S., YU H., SHIH C.-K., EBERT P., Surf. Sci., 518 (2002), 63.
[28] GAVIOLI L., KIMBERLIN K., TRINGIDES M., WENDELKEN J., ZHANG Z., Phys. Rev. Lett., 82 (1999), 129.
[29] HUANG L., CHEY S.J., WEAVER J., Surf. Sci., 416 (1998), L1101.
[30] MORESCO F., ROCCA M., HILDEBRANDT T., HENZLER M., Surf. Sci., 463 (2000), 22.
[31] JIANG C.-S., HASEGAWA S., INO S., Phys. Rev. B, 54 (1996), 10389.
[32] SATO N., TAKEDA S., NAGAO T., HASEGAWA S., Phys. Rev. B, 59 (1999), 2035.

[33] NAGAO T., HILDEBRANDT T., HENZLER M., HASEGAWA S., Phys. Rev. Lett., 86 (2001), 5747.
[34] WAN K., LIN A., NOGAMI J., Phys. Rev. B, 47 (1993), 13700.
[35] *Vacuum Physics and Technology*, Vol. 14, *Methods in Experimental Physics*, G.L. Weissler (Ed.), Academic Press, New York, 1979.
[36] KIRAKOSIAN A., BENNEWITZ R., CRAIN J.N., FAUSTER TH., LIN J.-L., PETROVYKH D.Y., HIMPSEL F.J., Appl. Phys. Lett., 79 (2001), 1608.
[37] HOQUE E., PETKOVA A., HENZLER M., Surf. Sci., 515 (2002), 312.
[38] HENZLER M., ZHACHUK R., Thin Solid Films, 428 (2003), 129.
[39] WANG X.-S., WEINBERG W.H., Surf. Sci., 314 (1994), 71.
[40] BASKI A.A., ERWIN S.C., WHITMAN L.J., Surf. Sci., 423 (1999), L265.
[41] BIERMANN S., GEORGES A., GIAMARCHI T., LICHTENSTEIN A. [in:] *Strongly Correlated Fermions and Bosons in Low Dimensional Disordered Systems*, I.V. Lerner, B.L. Althsuler, V.I. Falko, T. Giamarchi (Eds.), Kluwer, Dordrecht, 2002, p. 81.
[42] DRESSEL M., PETUKHOV K., SALAMEH B., ZORNAZA P., GIAMARCHI T., Phys. Rev. B, 71 (2005), 075104.
[43] GIAMARCHI T., SCHULZ H., Phys. Rev. B, 37 (1998), 325.
[44] GEORGES A., GIAMARCHI T., SANDLER N., Phys. Rev. B, 61 (2000), 16393.

Received 23 September 2004
Revised 16 November 2004